Engineered biomimetic nanoparticle for dual targeting of the cancer stem-like cell population in sonic hedgehog medulloblastoma

Jinhwan Kim[a,1], Abhinav Dey[b,1], Anshu Malhotra[b], Jingbo Liu[b], Song Ih Ahn[a,c], Yoshitaka J. Sei[a,c], Anna M. Kenney[b], Tobey J. MacDonald[b,2], and YongTae Kim[a,c,d,e,2]

[a]George W. Woodruff School of Mechanical Engineering, Georgia Institute of Technology, Atlanta, GA 30332; [b]Department of Pediatrics, Emory University, Atlanta, GA 30322; [c]Parker H. Petit Institute for Bioengineering and Bioscience, Georgia Institute of Technology, Atlanta, GA 30332; [d]Wallace H. Coulter Department of Biomedical Engineering, Georgia Institute of Technology, Atlanta, GA 30332; and [e]Institute for Electronics and Nanotechnology, Georgia Institute of Technology, Atlanta, GA 30332

Edited by Chad A. Mirkin, Northwestern University, Evanston, IL, and approved August 19, 2020 (received for review July 3, 2019)

The sonic hedgehog subtype of medulloblastoma (SHH MB) is associated with treatment failure and poor outcome. Current strategies utilizing whole brain radiation therapy result in deleterious off-target effects on the normal developing childhood brain. Most conventional chemotherapies remain limited by ineffective blood–brain barrier (BBB) penetrance. These challenges signify an unmet need for drug carriers that can cross the BBB and deliver drugs to targeted sites with high drug-loading efficiency and long-term stability. We herein leverage the enhanced stability and targeting ability of engineered high-density lipoprotein-mimetic nanoparticles (eHNPs) to cross the BBB and deliver a SHH inhibitor effectively to the cancer stem-like cell population in SHH MB. Our microfluidic technology enabled highly reproducible production of multicomponent eHNPs incorporated with apolipoprotein A1, anti-CD15, and a SHH inhibitor (LDE225). We demonstrate the dual-targeted delivery and enhanced therapeutic effect of eHNP-A1-CD15-LDE225 via scavenger receptor class B type 1 (SR-B1) and CD15 on brain SHH MB cells in vitro, ex vivo, and in vivo. Moreover, we show that eHNP-A1 not only serves as a stable drug carrier, but also has a therapeutic effect itself through SR-B1-mediated intracellular cholesterol depletion in SHH MB cells. Through the facilitated and targeted cellular uptake of drugs and direct therapeutic role of this engineered biomimetic nanocarrier in SHH MB, our multifunctional nanoparticle provides intriguing therapeutic promise as an effective and potent nanomedicine for the treatment of SHH MB.

medulloblastoma | high-density lipoprotein | cancer | nanoparticle | drug delivery

Treatment of medulloblastoma (MB), the most common malignant childhood brain tumor, includes surgery, whole brain and spine radiation, and chemotherapy, which leads to serious side effects, including profound neurocognitive deficits (1, 2), highlighting an urgent need for targeted drug delivery to MB cells. In particular, the sonic hedgehog subtype of MB (SHH MB), which represents ∼30% of MB, is associated with treatment failure and poor outcome in older children and those with metastatic disease (3, 4). Alternative strategies aimed at developing tumor-targeted therapies that effectively cross the blood–brain barrier (BBB) are thus critically needed for SHH MB.

One strategy for the treatment of SHH MB is to suppress the growth- and survival-promoting signaling cascades in the SHH pathway (e.g., use of antagonists for Smoothened [Smo]). However, the utility of SHH inhibitors for the treatment of SHH MB remains questionable mainly due to intrinsic and acquired drug resistance (5). An alternative therapeutic approach is to disrupt the regulation of intracellular cholesterol that is known to play an important role in activating the SHH pathway (6). In fact, cholesterylation of the SHH precursor is required to secrete SHH into the extracellular environment to trigger autocrine and paracrine signaling (7), followed by the binding of cholesterol to Smo, which in turn activates GLI transcriptional activity in the cell nucleus (8), indicating that SHH signaling is regulated through cholesterol homeostasis (9). A recent finding on the high expression of the cholesterol transporter, scavenger receptor class B type 1 (SR-B1) on SHH MB cells (10) further suggests the therapeutic potential and specificity of high-density lipoprotein (HDL) for the treatment of SHH MB due to SR-B1-mediated cholesterol transport and the role of cholesterol homeostasis in maintaining SHH pathway signaling for survival.

Brain tumors are extremely difficult to treat due to the limited permeability of the BBB, which significantly reduces the efficacy of systemic delivery of drugs to tumors within the brain (11–13). This indicates the importance of the development of novel, stable delivery carriers capable of effectively crossing the BBB and delivering sufficient drug loads to target sites. However, it remains difficult to achieve robust targeted delivery of sufficient

Significance

This study shows that an engineered biomimetic nanoparticle decorated with a targeting ligand and loaded with a sonic hedgehog inhibitor maintains its stability in the circulation, crosses the blood–brain barrier (BBB), and delivers drug molecules to the cancer stem-like cell population in sonic hedgehog subtype of medulloblastoma. Leveraging the natural capabilities of high-density lipoprotein, our nanoparticle enables the facilitated and targeted cellular uptake of drugs and receptor-mediated intracellular cholesterol depletion in medulloblastoma cells. Our successful in vivo validation of the nanocarrier performance suggests a new viable strategy by which to deliver other drugs that are reportedly unable to cross the BBB, have low bioavailability, and/or off-target effects for the treatment of brain tumors, including medulloblastoma.

Author contributions: J.K., A.D., T.J.M., and Y.K. designed research; J.K., A.D., A.M., J.L., S.I.A., Y.J.S., T.J.M., and Y.K. performed research; A.M.K., T.J.M., and Y.K. contributed new reagents/analytic tools; J.K., A.D., A.M., J.L., S.I.A., Y.J.S., T.J.M., and Y.K. analyzed data; J.K., A.D., T.J.M., and Y.K. wrote the paper; and A.M.K. provided insightful comments in the overall project.

Competing interest statement: In compliance with the institutional guidelines of the Georgia Institute of Technology, Y.K. discloses his financial interest in Mepsgen and Mepsgenlab, two biotechnology companies developing microengineered physiological systems and biomimetic nanoparticles for medical applications. Mepsgen and Mepsgenlab did not support the aforementioned research, and currently these companies have no rights to any technology or intellectual property developed as part of this research.

This article is a PNAS Direct Submission.

[1]J.K. and A.D. contributed equally to this work.

[2]To whom correspondence may be addressed. Email: tobey.macdonald@emory.edu or ytkim@gatech.edu.

This article contains supporting information online at https://www.pnas.org/lookup/suppl/doi:10.1073/pnas.1911229117/-/DCSupplemental.

First published September 15, 2020.

therapeutic agents to brain tumors with prolonged stability (14, 15). This is largely due to the lack of delivery vehicles simultaneously capable of high drug loading efficiency, high targeting efficiency, and robust stability that can also cross the BBB. Furthermore, conventional approaches to synthesis of delivery carriers through macroscopic mixing of precursor solutions have faced challenges including high batch-to-batch variations in the physicochemical properties and difficulties in scaling up the production (16, 17).

Taking advantage of unique physicochemical properties, multifunctional nanocarriers have demonstrated the capability to deliver drugs to targeted sites and overcome drug resistance in several types of cancer (18, 19). In particular, HDL, a highly stable endogenous nanoparticle that has significant roles in several biological events, including reverse cholesterol transport (RCT) and antiinflammatory effects (20, 21), has been proposed as a promising nanocarrier for targeted delivery of therapeutic molecules with high stability [up to 24 h half-life (22)]. Apolipoprotein A1 interacts with several receptors on brain endothelial cells as well, enabling the transport of HDL nanoparticle and subsequent release of loaded cargos into the brain parenchyma through receptor-mediated transcytosis (23, 24). However, the structural and functional heterogeneity of endogenous HDL purified from human plasma may lead to unreproducible and unpredicted outcomes upon systemic administration for drug delivery (25, 26). Therefore, there has been a strong need to reconstitute the function of HDL nanoparticles with high homogeneity in structure, as well as the capability to incorporate therapeutic and diagnostic agents. Herein, we report a strategy applying engineered HDL-mimetic nanoparticles (eHNPs) for targeted delivery and enhanced therapeutic efficacy of the Smo inhibitor, sonidegib (LDE-225), in SHH MB cells. Our study demonstrates that eHNPs, like HDL nanoparticles that are reportedly able to get into the brain by crossing the BBB through SR-B1 and SNARE-mediated transcytosis (23), deliver therapeutics more effectively into the brain to exert an antitumor effect in SHH MB (Fig. 1).

Results

Microfluidic Synthesis and Characterization of eHNPs. With our microfluidic technology enabling a simple and facile single-step reconstitution of eHNPs with high homogeneity and reproducibility (*SI Appendix*, Fig. S1) (27, 28), we are able to not only produce the nanoparticles with high uniformity, but also decorate an antibody of the murine SHH MB cancer stem-like cell target, stage-specific embryonic antigen-1 (SSEA-1$^+$) or CD15 (*SI Appendix*, Fig. S2), on the surface of eHNP-A1 while incorporating LDE-225 into the nanoparticle core (Fig. 2*A*). Four different types of eHNPs were synthesized to evaluate the effect of each component (*SI Appendix*, Table S1). The synthesized eHNP-A1 exhibited a homogeneous discoidal shape of 13 nm in size (Fig. 2 *B* and *C*), like natural pre-beta HDL (29). Incorporation of CD15 into eHNP-A1 slightly increased the size to 15 nm (Fig. 2*B*), while maintaining the discoidal shape (Fig. 2*C*). Loading of LDE225, a hydrophobic drug used to treat MB by inhibiting hedgehog signaling (30), into the core of eHNP-A1 led to a large spherical particle with a size up to 25 nm (Fig. 2 *B* and *C*). The nanoparticle shell formed by apolipoprotein A1 and lipid resulted in a greater structural stability than lipid micelles while keeping LDE225 in the hydrophobic core. The target nanoparticle of eHNP-A1-CD15-LDE225 exhibited a similar size distribution with a slightly larger peak of 28 nm with a spherical shape. Our composition analysis showed that the high amounts of LDE225 in eHNP-A1-LDE225 and eHNP-A1-CD15-LDE225 were 7.2% (wt/wt) and 5.7% (wt/wt), respectively (Table 1 and *SI Appendix*, Fig. S3), owing to the structural stability provided by the scaffold protein apolipoprotein A1.

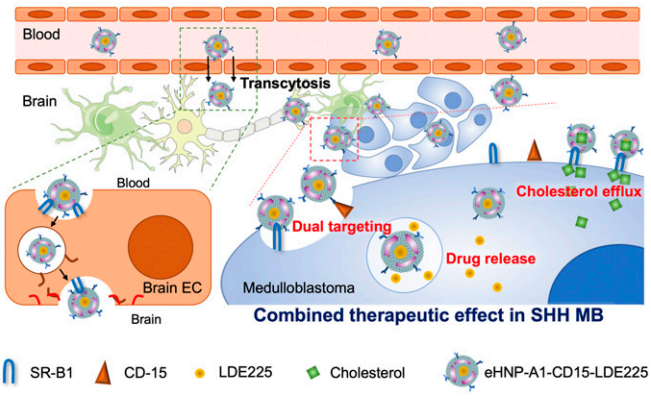

Fig. 1. Schematic illustration of engineered biomimetic nanoparticles for dual targeting of the cancer stem-like cell population in sonic hedgehog medulloblastoma (SHH MB) through receptor-mediated transcytosis across the blood-brain barrier (BBB) and subsequent receptor-mediated cellular internalization of engineered high-density lipoprotein-mimetic nanoparticle with anti-CD15 and LDE225 (eHNP-A1-CD15-LDE225) in SHH MB for drug release and cellular cholesterol efflux.

eHNP as a Delivery Carrier Capable of Crossing the Intact BBB to SHH MB. We first confirmed that eHNP-A1 can cross the BBB and get into the brain parenchyma with the accumulation of eHNP-A1 in the brain observed for 24 h after i.v. injection (Fig. 3*A* and *SI Appendix*, Fig. S4). Before we tested the ability of our target nanoparticle with multiple components to cross the BBB and deliver drugs to the targeted sites in the brain, we first investigated whether the BBB is intact and maintains the barrier function predicted in an in vivo brain tumor model of a SmoA1 MB tumor-bearing mouse. The SmoA1 mice were crossed with Math1-GFP to generate homozygous *SmoA1*$^{+/+}$:*Math1-GFP*$^{+/+}$ strain. These mice spontaneously develop tumors and were used between 4 and 6 mo of age (31). Tumor-bearing mice were identified with symptoms of enlarged posterior fossa, head tilt, ataxia, and hunched posture. After confirming the tumor growth, i.v. injections of Hoechst dye and Alexa-594 conjugated lectin in SmoA1-GFP tumor-bearing mice resulted in the localization of the Hoechst dye/Lectin-594 (red) in the areas near the vasculature, and its absence from the bulk of the tumor (green) (Fig. 3 *B* and *C*), in contrast to a widespread distribution in liver tissue sections from the same tumor-bearing mice (Fig. 3*D*). This result confirmed that the SmoA1 mouse MB model has an intact BBB, as was previously shown by others in a different murine MB model (32). We then confirmed the ability of eHNP-A1 to cross the intact BBB and accumulate in the MB cells of the SmoA1-GFP-MB-bearing mouse model upon i.v. injection (Fig. 3 *E*, *Upper*).

eHNPs Demonstrate Receptor-Facilitated Delivery into SHH MB. Like natural HDL, our eHNP-A1 may interact with several receptors, including SR-B1 on brain endothelial cells, enabling the release of loaded cargos into the brain parenchyma through receptor-mediated transcytosis (Fig. 1). We evaluated the cytosolic internalization of eHNPs facilitated by several receptors on SHH MB cells using confocal microscopy (Fig. 4*A* and *SI Appendix*, Fig. S5). Anti-CD15 incorporation into eHNP-A1s (eHNP-A1-CD15 and eHNP-A1-CD15-LDE225) enhanced cellular internalization up to four times greater than that of eHNP-A1, owing to the "dual targeting" receptor-mediated uptake by CD15 and SR-B1. In addition, cytosolic internalization of eHNP-A1-CD15-LDE225 was significantly reduced upon pretreatment with block lipid transporter-1 (BLT-1), a known inhibitor of SB-B1, and excess free anti-CD15, further demonstrating that dual SR-B1- and CD15-mediated cellular uptake led to the efficient cellular delivery of the eHNPs (Fig. 4*B* and *SI Appendix*, Fig. S6).

We then probed the targeting efficiency of the eHNPs in the brain tumor microenvironment, especially to the CD15-positive

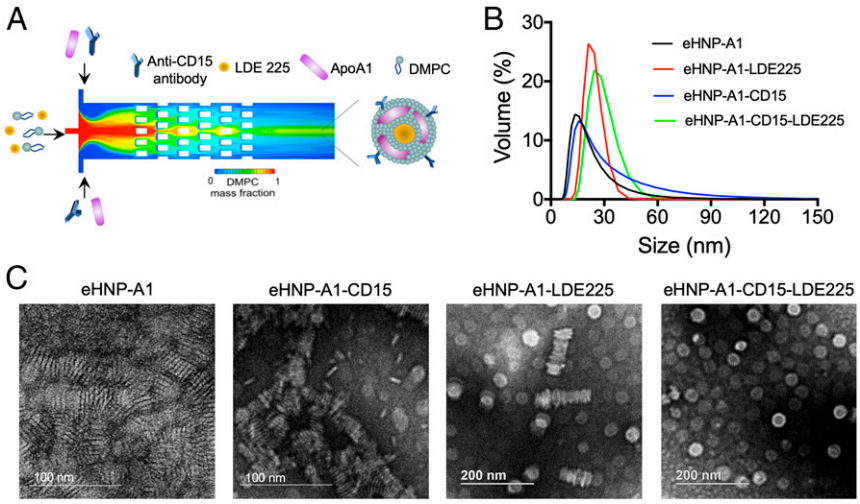

Fig. 2. Synthesis and characterization of eHNPs for the delivery of SHH inhibitors in SHH MB. (*A*) Schematic illustration of the synthesis of eHNP-A1-CD15-LDE225 in a three-inlet microfluidic device. (*B*) Hydrodynamic volume and (*C*) transmission electron microscopy (TEM) image of eHNP-A1-CD15-LDE225 and its derivatives.

cancer stem-like cells. We standardized the culture conditions for the growth of SmoA1 organotypic tumor slice cultures ex vivo to analyze the effect of antitumor agents in the tumor microenvironment (33). We evaluated the targeting effect of eHNP-A1-CD15-LDE225 and its derivatives on ex vivo organotypic slice cultures (Fig. 4*C*). The slice cultures tagged with anti-CD15 (eHNP-A1-CD15) exhibited more localization in the perivascular niche areas of tumor tissues when compared to anti-CD15-free eHNPs (eHNP-A1 and eHNP-A1-LDE225). Subsequently, we i.v. administered eHNP-A1-CD15 to the SmoA1-GFP tumor-bearing mice and examined the cryosectioned tissues under a confocal microscope in a time-dependent manner (*SI Appendix*, Fig. S7). In order to visualize the preferential localization of eHNPs targeting the cancer stem cells within the tumor microenvironment, we first carried out CD15 immunofluorescence staining for cancer stem cells in MB tissue slices and confirmed the higher expression of CD15 in the perivascular areas (Fig. 4 *D*, *Upper*), as previously reported by other groups that endothelial cells interact closely with self-renewing brain tumor cells and secrete factors that maintain these cells in a stem cell-like state (Fig. 4*D*). Both CD15 and eHNP-A1-CD15 colocalize to the perivascular space (Fig. 4 *D* and *E*, *Lower*), whereas other non-anti-CD15-conjugated eHNPs are more diffusely distributed (Figs. 3*E* and 4*C*), indicating the targeting effect directed to the stem cell population. Some of the heterogeneous distribution in these images are in part due to the SR-B1-mediated uptake on all MB cells. This result is in agreement with the localization of CD15 antigen in the cancer stem-like cell niche of the brain tumor tissue (Fig. 4*D*) in the murine medulloblastoma, whereas eHNP-A1-CD15 showed a nontargeted distribution in the liver tissue sections (Fig. 4 *E*, *Upper*). Taken together, these results confirmed the ability of the eHNPs to traverse the BBB and target cancer stem-like cell populations in the SmoA1 mouse model of medulloblastoma through dual targeting of cells that are both CD15-positive and demonstrate high expression of SR-B1.

eHNP-A1-CD15-LDE225 Markedly Enhances LDE225 Inhibition of SHH MB. With the successful BBB penetration and subsequent efficient targeting of SHH MB cells, we next investigated the therapeutic efficacy of eHNP-A1-CD15-LDE225 and its derivatives. To confirm the effect of each component in the proposed nanoparticles, we treated SHH MB cells (DAOY and PZp53) with free LDE225, eHNP-A1, eHNP-A1-CD15, eHNP-A1-LDE225, and eHNP-A1-CD15-LDE225, and monitored the cell viability (Fig. 5*A* and *SI Appendix*, Fig. S8). Compared to LDE225 treatment, which exhibited dose-dependent inhibition of cell viability (IC50 ~2 μM), eHNP-A1-LDE225 treatment dramatically enhanced the therapeutic efficacy (IC50 ~70 nM). Furthermore, the addition of targeting capability using anti-CD15 (eHNP-A1-CD15-LDE225) remarkably led to 250-fold reduction of the IC50 value (~8 nM). More interestingly, eHNP-A1 and eHNP-A1-CD15 without drug loading also exhibited marked therapeutic effects; the cell viability following treatment with eHNP-A1 and eHNP-A1-CD15 decreased to 63%, equivalent to a treatment concentration corresponding to 10 μM LDE225, indicating that the eHNP-A1 alone has a therapeutic potential for the treatment of SHH MB, which was also supported by a recent study (10).

The enhanced therapeutic effect of eHNP-A1-CD15-LDE225 shown in SHH MB cells was further investigated using a specific inhibitor of the HDL receptor SR-B1, BLT-1, which mediates bidirectional flow of cholesterol in and out of cells, as well as free anti-CD15 (Fig. 5 *B–D* and *SI Appendix*, Fig. S9). Pretreatment with anti-CD15 affected the viability for cells treated with eHNP-A1-CD15-LDE225, but not for cells treated with free LDE225

Table 1. Composition of eHNP-A1-CD15-LDE225 and its derivatives. ND: not determined

	eHNP-A1	eHNP-A1-CD15	eHNP-A1-LDE225	eHNP-A1-CD15-LDE225
ApoA1	59.4%	40.0%	55.6%	42.4%
CD15	ND	28.3%	ND	23.8%
LDE225	ND	ND	7.2%	5.7%
DMPC	40.6%	31.7%	37.2%	28.1%
Shape	Discoidal	Discoidal	Spherical	Spherical

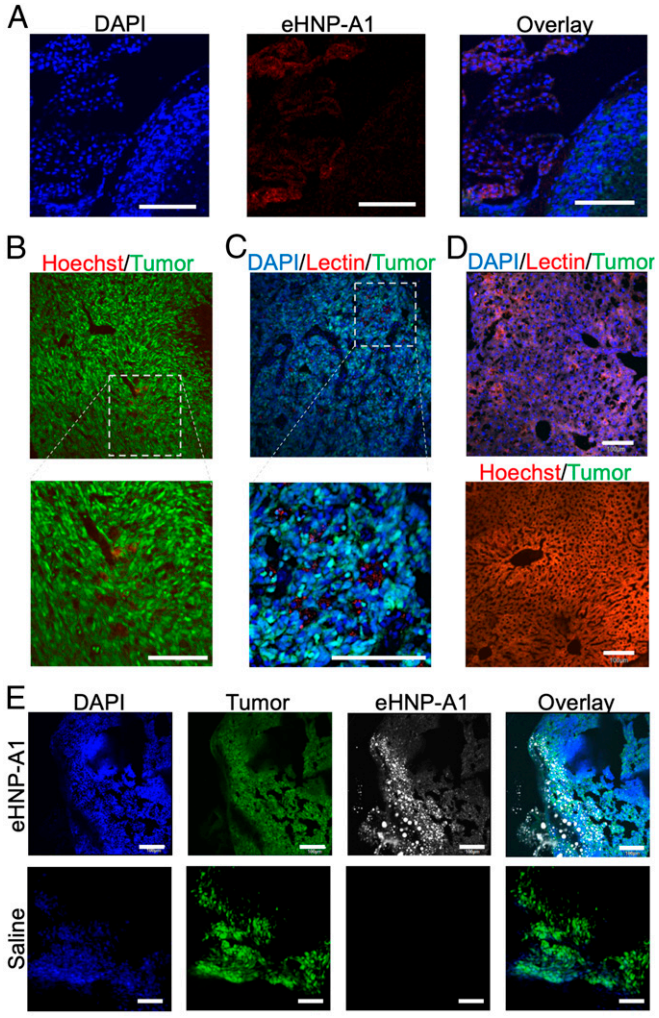

Fig. 3. eHNPs can cross the intact BBB and accumulate in and around the SHH MB cells in a SHH MB mouse model. (*A*) Brain slice of an eHNP-A1-injected mouse. Blue represents nucleus; red represents eHNP-A1. (*B* and *C*) Intact BBB in GFP-expressing MB-bearing mice is demonstrated by the minimal perfusion of Hoechst dye in the brain after the systemic injection. (*D*) Distinct high widespread perfusion of Hoechst in the liver. (*E*) Localization of eHNP-A1 in the GFP-expressing MB cells in a SHH MB mouse model upon i.v. injection (nucleus in blue, SmoA1 mouse MB cells in green, and eHNP-A1 in white). (Scale bars, 100 μm.)

and eHNP-A1, indicating that CD15 on SHH MB facilitates the uptake of eHNP-A1-CD15-LDE225 to SHH MB cells and contributes to the therapeutic effect. Importantly, pretreatment of DAOY cells with BLT-1 significantly further reduced the efficacy of eHNP-A1 and eHNP-A1-CD15-LDE225, suggesting that SR-B1 not only promotes the interaction of eHNPs with SHH-MB cells, but may also mediate eHNP-induced dysregulation of cholesterol homeostasis within the DAOY cells, which in turn further inhibits SHH signaling pathway. In contrast, following treatment with free LDE225, BLT-1 pretreatment showed only a minimal effect on cell viability, possibly because the blockade of lipid transport by BLT-1 may also affect the Smo pathway which is highly dependent on lipid metabolism. Moreover, we confirmed from a drug release test that acidic pH contributed to a higher drug release (*SI Appendix*, Fig. S10), indicating that the release of LDE225 partly occurs inside the endosome. The blocking of endosomal acidification using bafilomycin A1 (Baf A1) significantly lowered the therapeutic effect of eHNP-A1-CD15-LDE225, whereas there was an insignificant effect of Baf A1 on free LDE225. This result further demonstrates that the drug releases within the cell, more specifically inside the endosome during the endosomal acidification (*SI Appendix*, Fig. S11). We also found that the transport mechanism of LDE225 into the cell is collaborative: endocytosis and consequent release upon acidification, and SR-B1-mediated transport bypassing endocytic pathway (*SI Appendix*, Fig. S12).

Based on the striking inhibition of cell viability observed following treatment with eHNPs in the absence of SR-B1 blockade, we hypothesized that eHNPs enable not only the efficient delivery of LDE225 into the cells, but also enhance the therapeutic effect through mediating the transport of cholesterol out of cells, which is supported by studies demonstrating the critical role of cholesterol in SHH signaling in SHH subtype cells (6–8). To prove this hypothesis, we evaluated the cholesterol efflux in DAOY cells after treatment with the eHNPs (Fig. 5*E*). DAOY cells treated with eHNP-A1, eHNP-A1-CD15, and eHNP-A1-CD15-LDE225 exhibited much higher cholesterol efflux than nontreated and free LDE225-treated cells. Interestingly, eHNP-A1-CD15-LDE225 showed less cholesterol efflux than that of eHNP-A1 and eHNP-A1-CD15, probably due to the limited room of the nanoparticle core that was loaded with LDE225, despite promoting significantly higher cholesterol transport out of SHH-MB cells compared to nontreated or free LDE225-treated cells.

To ascertain the capability of these eHNPs to cause tumor cell death ex vivo, we first maintained the organotypic tumor slice cultures in the presence of eHNPs and then stained for the cell death marker cleaved-caspase 3 (CC3). A higher CC3 staining (blue) in slice cultures treated with eHNP-A1s containing LDE225 was observed than in non-LDE225-treated ones (*SI Appendix*, Figs. S13 and S14). To further demonstrate the ability of the nanoparticles to deliver drugs in the murine brain tumors in vivo, we i.v. injected eHNP-A1-CD15-LDE225 and its derivatives to MB-bearing mice and monitored the therapeutic efficacy. We employed two different mouse models of SHH MB, which are the SmoA1-GFP model and Patched (PTC) knockout model. Long-term magnetic resonance imaging (MRI) scans of the tumor growth in both SHH MB models treated by the eHNP-A1-CD15-LDE225-treated group exhibited the well-maintained cerebellum structure and minimal tumor growth, whereas the saline-treated group showed a disrupted cerebellum structure, a blunted edge of lobes, and an outstanding tumor growth (Fig. 5*F* and *SI Appendix*, Fig. S15). The volume of SHH MB (PTC) was reduced by 72% in the eHNP-A1-CD15-LDE225-treated group, whereas the saline-treated group showed a 4.3-fold increase in the tumor volume (Fig. 5*G*), resulting in a markedly lower tumor growth rate and significantly longer survival in the eHNP-A1-CD15-LDE225-treated group than those of the control group (Fig. 5*H* and *SI Appendix*, Fig. S16). Similarly, in the other SHH MB-bearing SmoA1-GFP model, tumor growth was significantly inhibited in the eHNP-A1-CD15-LDE225-treated group than that of the saline-treated group, and the eHNP-A1-CD15-LDE225-injected group exhibited significantly enhanced survival rate than the control group, further demonstrating the efficient treatment of SHH MB (*SI Appendix*, Fig. S17). In order to prove the biological activity of eHNP-A1-CD15-LDE225 and its derivatives, we treated samples to SmoA1-GFP mice and subsequently sectioned and immunostained the tissues for CC3 (Fig. 5 *I* and *J*). For eHNP-A1-LDE225 and eHNP-A1-CD15-LDE225, CC3 expressions were high in the brain tumor regions (GFP-positive), demonstrating the effective targeted delivery of LDE225 to the cancer cells in vivo. Interestingly, in a good correlation with in vitro studies, eHNP-A1 and eHNP-A1-CD15 also resulted in a greater degree of CC3 activation than negative control, whereas the degree was much less than that of LDE225-loaded nanoparticles, revealing that the effective cholesterol efflux by eHNPs led to more effective therapeutic outcome in

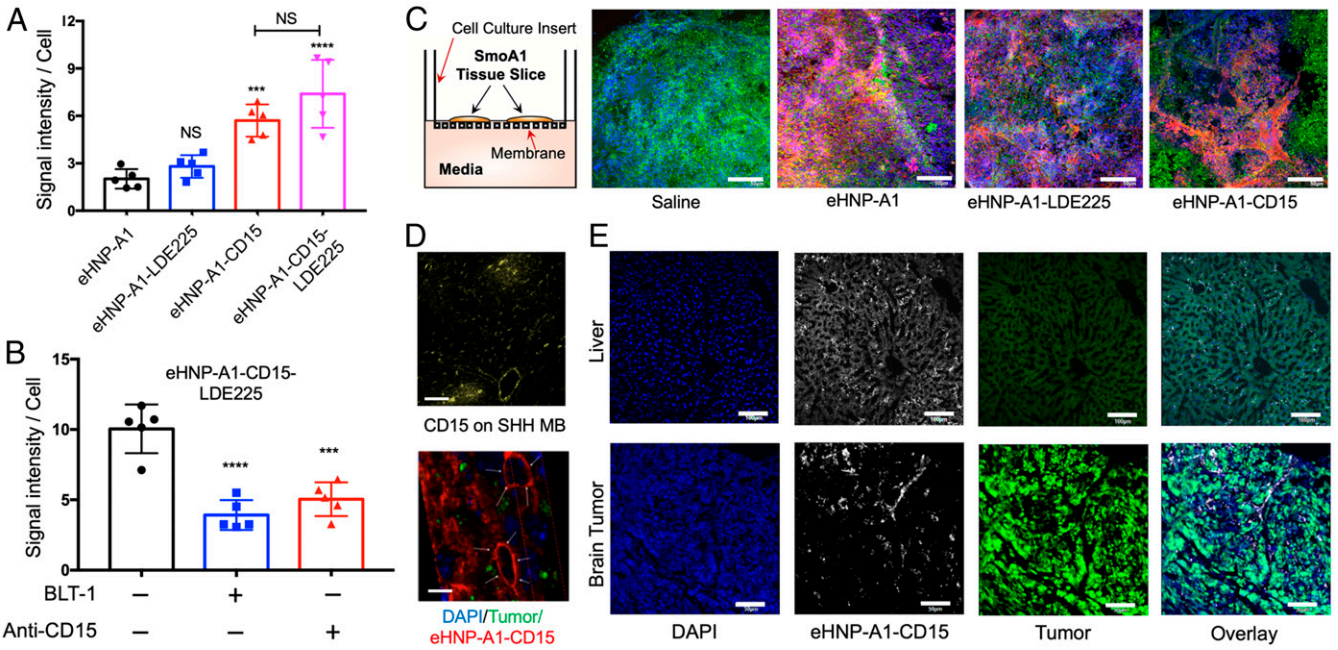

Fig. 4. Receptor-facilitated delivery of eHNP-A1-CD15-LDE225. (*A*) Quantitative cellular internalization of eHNP-A1-CD15-LDE225 and its derivatives in DAOY cells in vitro. All statistical analyses are against the eHNP-A1-treated group. (*B*) Quantitative internalization of eHNP-A1-CD15-LDE225 upon the treatment of inhibitors in DAOY cells in vitro. Statistical analyses are against –BLT-1/–anti-CD15. (*C*) Image of GFP-expressing SmoA1 MB organotypic tumor slice culture upon the treatment of eHNP-A1-CD15-LDE225 and its derivatives ex vivo: from left to right, schematic for organotypic slice cultures; nontreated; eHNP-A1-treated; eHNP-A1-LDE225 treated; and eHNP-A1-CD15 treated. (Scale bar, 100 μm.) (*D*) Immunofluorescence staining of CD15 in cryosectioned Smo-A1 MB (*Upper*) and high-resolution confocal-based 3D-image reconstruction of the localization of eHNP-A1-CD15 along the perivascular niche area (arrows) in organotypic slice cultures (*Bottom*). (Scale bars, 50 μm.) (*E*) Penetration of the BBB and restricted localization in vivo of eHNP-A1-CD15 in the perivascular niche of GFP-expressing SmoA1 MB-bearing mice (*Lower*), and nonrestricted distribution of eHNP-A1-CD15 in the liver (*Upper*) upon i.v. injection. Blue represents nucleus; green represents SmoA1 mouse MB cells; white represents eHNP-A1. (Scale bars of *Upper* and *Lower* is 100 and 50 μm, respectively.) (***$P < 0.001$, ****$P < 0.0001$, NS: not significant.)

SHH MBs reducing the drug dosage. Moreover, additional apoptosis markers including terminal deoxynucleotidyl transferase dUTP nick end labeling (TUNEL) and cleaved poly (ADP ribose) polymerase (PARP) confirmed our findings with well-correlated images and quantitative results (Fig. 5*J* and *SI Appendix*, Figs. S18 and S19). Moreover, we identified spinal cord samples with GFP-positive regions to locate metastatic sites of SmoA1 tumors as reported previously (34). Interestingly, we also found the targeted delivery of the nanoparticle payload to all metastatic sites, compared to a minimal level in the liver tissue from the same group of SmoA1-treated mice (*SI Appendix*, Fig. S20). Targeted in vivo delivery of the LDE225 to the primary and metastatic tumors was further supported by negligible LDE225 release from eHNPs at neutral pH or a serum-containing environment (*SI Appendix*, Fig. S11). Taken all together, our findings clearly demonstrated that our multifunctional HDL-mimetic nanoparticles can serve as an efficient and potent nanomedicine by facilitating cellular uptake and by exploiting cholesterol transport, a critical factor in SHH MB.

Discussion

Radiation continues to be the mainstay of treatment for MB, in part due to the limited ability of conventional chemotherapies to effectively cross the BBB; however, this therapy results in significant deleterious off-target effects on the childhood brain (35). Meanwhile, the use of tumor-targeting agents, such as SHH inhibitors for SHH MB have shown high efficacy, but resistance develops too quickly, and are ineffective for more than half of the patients harboring mutations downstream of the Smo target (36). In the present study, we addressed these challenges by using an engineered biomimetic nanoparticle that maintains its stability in the circulation, effectively crosses the BBB, and delivers drug molecules to the cancer stem-like cell population for the treatment of SHH MB.

A variety of materials have been used to formulate nanomedicines for drug delivery and imaging applications, most of all, natural nanoparticles like HDL, which due to their endogenous character and reliable stability in circulation, are well suited as a vehicle for targeted delivery of therapeutic or diagnostic agents. However, the continuous remodeling and interchange of HDL components generates a highly heterogeneous population of HDL in terms of size, composition, and functionality. Purified HDL particles from human blood consist of various apolipoproteins and multiple lipid derivatives with different sizes and compositions, resulting in low reproducible therapeutic outcomes (37, 38). To overcome these challenges, HDL-based nanomaterials have been reconstituted to carry inorganic nanocrystals as contrast agents for medical imaging as well as to serve as delivery vehicles for siRNAs or therapeutic molecules (39). However, these reconstitution approaches require multistep processes, which are highly dependent on synthetic conditions, difficult to scale up, and laborious, resulting in inevitable batch-to-batch variations and low reproducibility. In the present study, our microfluidic synthesis approach leveraging highly controlled microvortex mixing allows for the customizable assembly of eHNPs with enhanced functionality from multicomponent contributions of this complex nanoparticle platform (27, 28). This selective customization technology can be extended to a parallelized microvortex reactor array for scalable manufacturing of eHNPs to efficiently create a library of eHNPs (polydispersity index [PDI] < 0.1: highly homogeneous) (40). Our microfluidic technology for nanoparticle formulation processes provide effective control of the formation and characteristics of nanomaterials, leading to a narrow size distribution and high batch-to-batch reproducibility. With this advanced technology, we were able to engineer HDL-mimetic nanoparticles

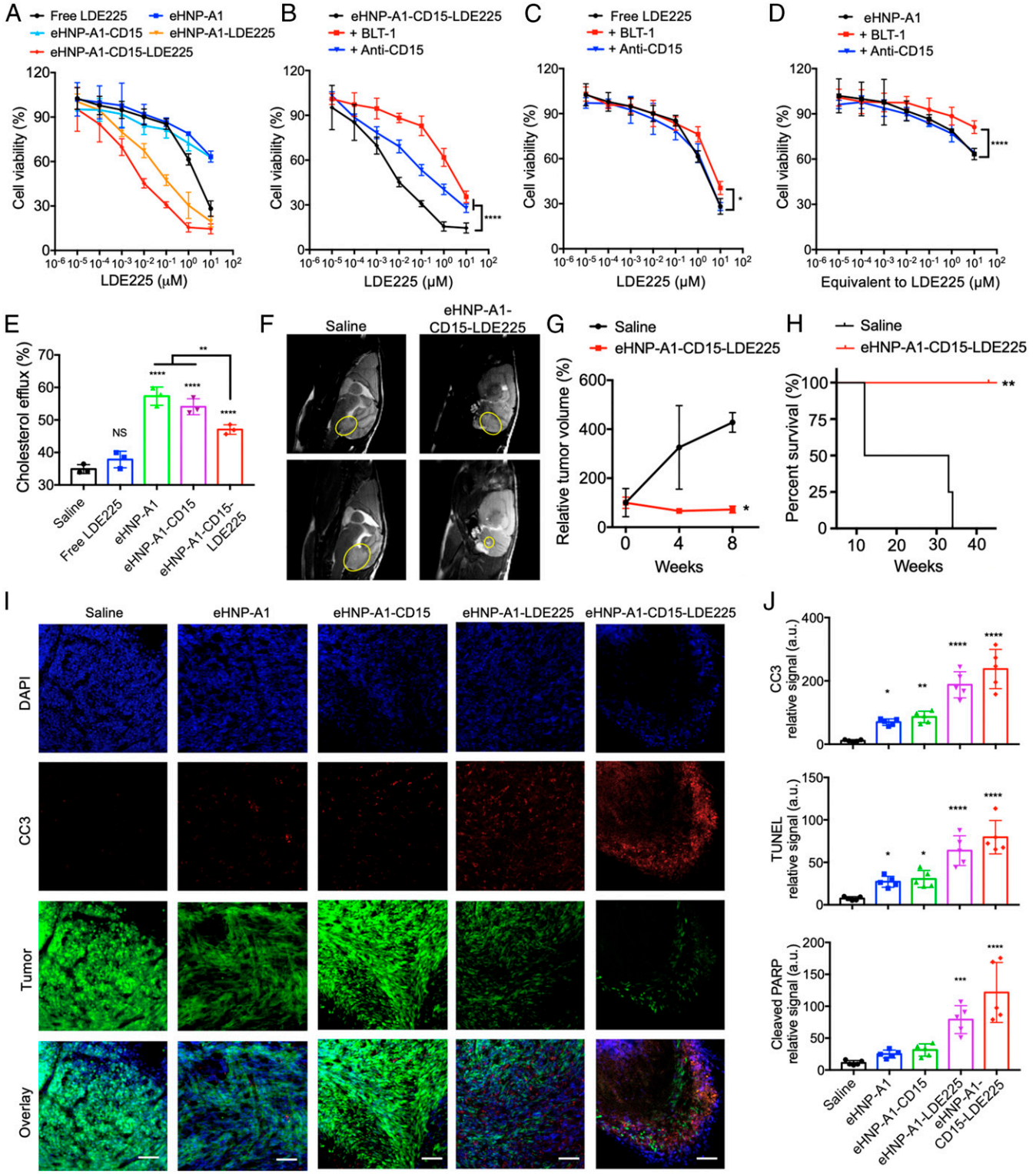

Fig. 5. Therapeutic effect of eHNP-A1-CD15-LDE225 in SHH MB. (*A*) In vitro cell viability of eHNP-A1-CD15-LDE225 and its derivatives in DAOY cells. (*B–D*) Cell viability of DAOY cells treated with (*B*) eHNP-A1-CD15-LDE225, (*C*) free LDE225, and (*D*) eHNP-A1 in the presence of treatment with BLT-1 or free anti-CD15. (*E*) Cholesterol efflux assay upon treatment with eHNP-A1-CD15-LDE225 and its derivatives in DAOY cells. (*F*) MRI scans of MB-bearing PTC mice brain before and 4 wk after the i.v. injection of saline and eHNP-A1-CD15-LDE225. Tumor region is circled in yellow. (*G*) Relative tumor volume of MB before and after the injection of saline and eHNP-A1-CD15-LDE225. (*H*) Percent survival of SHH MB-bearing PTC mice injected with saline and eHNP-A1-CD15-LDE225. (*I*) Penetration of the BBB and subsequent therapeutic effect in vivo of eHNP-A1-CD15-LDE225 and its derivatives in the GFP-expressing MB-bearing SmoA1 mice upon i.v. injection (nucleus in blue, SmoA1 mouse MB cells in green, CC3 activation in red). (Scale bar, 100 μm.) (*J*) Quantitative apoptosis analysis of eHNP-A1-CD15-LDE225 and its derivatives in the SmoA1-GFP mouse MB cells in vivo. Quantitative results of CC3 activation (*Top*), TUNEL assay (*Middle*), and PARP activation (*Bottom*). All statistical analyses are against the saline-treated group. (*$P < 0.05$, **$P < 0.01$, ***$P < 0.001$, ****$P < 0.0001$, NS: not significant).

and exploit the robust stability and BBB-traversing ability of natural HDL in our body (23). With the high homogeneity of our eHNPs, we can expect the highly reproducible therapeutic outcomes for further clinical translations.

Cholesterol plays several crucial roles in SHH MB cells, and thus the level of intracellular cholesterol is maintained at a higher concentration than other cell types to activate the SHH pathway (9). Taking advantage of HDL's primary function of transporting cholesterol in our body, we have demonstrated the use of eHNP as an efficient cholesterol transporter from the cytoplasm of SHH MB cells to the extracellular region. The depletion of intracellular cholesterol in SHH MB cells led to the cytotoxicity observed, presumably by inhibiting the SHH pathway, confirming the potential of eHNP-A1-CD15-LDE225 as not only a robust delivery vehicle of therapeutic molecules across the BBB, but also as a therapeutic agent itself that could also potentially counteract resistance. The enhanced efficacy attributed by eHNP also suggests the potential of minimizing the systemic dose of other chemical drugs that are detrimental if nonspecifically released during the circulation.

In summary, we presented a design of BBB-penetrant biomimetic nanoparticles decorated with a targeting ligand (anti-CD15) and loaded with a SHH inhibitor (LDE225). Microfluidic technology enabled the continuous formation of highly homogenous eHNPs. These nanoparticles show the ability to cross the BBB in SHH MB in vivo and deliver the payload effectively to all sites of disease in a highly targeted manner. With the successful in vivo validation of the platform using our eHNPs, this study suggests a viable strategy by which to deliver many other chemical drugs that are reportedly unable to cross the BBB, have low bioavailability, or systemic and off-target effects. Our study demonstrated advanced approaches to the development of biomimetic nanocarriers capable of crossing the BBB and delivering drugs to the dual-targeted tumor cells, including specific targeting of the cancer stem-like cell population. Although the nanocarrier targeting model presented is to test the proof of concept in vivo, and so may be limited in direct human translation due to SSEA-1/CD15 being present on blood cells, our model will provide a nanomedicine platform that enables preclinical drug testing and screening for MB in vivo.

Materials and Methods

Preparation of Nanoparticles. A three-inlet microfluidic device that creates propagating microvortices was used for a single-step, continuous, and self-assembly-based synthesis of eHNP-A1-CD15-LDE225. Briefly, an organic phase comprising 2.75 mg/mL of 1,2-dimyristoyl-sn-glycero-3-phosphocholine (DMPC, Avanti Polar Lipids), 0.3 mg/mL of 1,1′-dioctadecyl-3,3,3′,3′-tetramethylindodicarbocyanine (DiD), and 0.2 mg/mL of LDE225 in absolute ethanol was introduced into the center inlet of the microfluidic device at a flow rate of 0.8 mL/min. An aqueous phase consisting of 0.2 mg/mL of apolipoprotein A1 (Millipore Sigma) and 0.05 mg/mL of anti-CD15 (BD Biosciences) in phosphate buffered saline (PBS) (pH = 7.4) was introduced into two outer inlets at a rate of 2.2 mL/min. Each of the organic and aqueous phases was injected using a programmable syringe pump (Harvard Apparatus) with the desired flow rates. After running the syringe pump, the mixture solution from outlet was collected and transferred to a centrifugal membrane filter (EMD Millipore) with a molecular weight cutoff (MWCO) of 50,000, and purified three times in PBS at a speed of 3,900 rpm for 20 min. Synthesized eHNP-A1-CD15-LDE225 was stored in PBS at 4 °C for further usage.

Characterization of Nanoparticles. The hydrodynamic volumes of samples were obtained by a Zetasizer Nano (Malvern Instrument). Size and morphology of samples were taken from a transmission electron microscope (TEM) (Hitachi 7700) at 120 kV coupled with the Digital Micrograph camera and software suite from Gatan. The amount of whole protein in a nanoparticle was quantified by bicinchoninic (BCA) assay according to the manufacturer's protocol, and the contents of anti-CD15 was quantified by measuring the fluorescence using the excitation/emission wavelengths of 496/578 nm. Drug loading contents were obtained by measuring the absorbance at 325 nm and subtracting the absorbance with the same amount of apolipoprotein A1 in the nanoparticle.

Cell Culture and Nanoparticle Treatment In Vitro. DAOY human MB cells were obtained from the ATCC. PZp53 cells were provided by Matthew P. Scott, School of Medicine, Stanford University, Stanford, CA. DAOY and PZp53 cells are Shh activated and *TP53* mutated. DAOY cells were seeded at 8×10^3 cell/well in 96-well plates overnight and seven different concentrations of LDE225 (0.00001, 0.0001, 0.001, 0.01, 0.1, 1, and 10 μM) were added in 200 μL total culture medium to each well for 48 h. For testing nanoparticles on DAOY and PZp53 cells, four different groups of newly synthesized nanoparticles (eHNP-A1, eHNP-A1-CD15, eHNP-A1-LDE225, and eHNP-A1-CD15-LDE225) were added to the media at the same concentrations (corresponding to 0.00001, 0.0001, 0.001, 0.01, 0.1, 1, and 10 μM LDE225). Cell viability was analyzed using the 3-(4,5-dimethylthiazol-2-yl)-2,5-diphenyltetrazolium bromide (MTT) assay (Sigma-Aldrich).

Cell Viability Assay. DAOY cells were seeded on 96-well plates at an initial density of 8×10^3 cell/well and incubated overnight. Before the treatment of samples, cells were preincubated with 200 μM of block lipid transporter-1 (BLT-1) or 10 μM of free anti-CD15 for 30 min. Cells were then washed and replaced with total culture medium containing (or corresponding to) 0.00001, 0.0001, 0.001, 0.01, 0.1, 1, and 10 μM LDE225 and incubated for 48 h. Cell viability was measured using the aforementioned MTT assay.

Mouse Tumor Model. All mouse model experiments were carried out in compliance with the Emory University Institutional Animal Care and Use Committee (IACUC) guidelines using Emory IACUC approved protocols. For the ex vivo and in vivo experiments, SmoA1 Transgenic (Jax 008831) and Math-Cre-ER-Ptch flox/flox were used. For the Math-Cre-ER-Ptch flox/flox mice, the pregnant female mice were administered tamoxifen (T-5648, Sigma) by oral gavage using 24-G gavaging needles (Fine Science Tools) after embryonic day 17 (E17.0) to induce MB formation. Tamoxifen was prepared as a 20 mg/mL solution in corn oil (Sigma) and tamoxifen doses were 4.0 mg/200 μL for treatment of pregnant females. After the pups were weaned and reached 5 wk old, the development of tumor was confirmed by MRI and mice were enrolled in the study.

Tumor Slice Cultures and Nanoparticle Treatment Ex Vivo. SmoA1 mice were anesthetized using CO_2 inhalation, the GFP-positive tumor tissue was removed, and tissue was embedded in 4% agarose in 1× Hanks' Balanced Salt Solution (HBSS) supplemented with 6 g/L dextrose. Tumors were sectioned horizontally into 300-μm-thick slices with a vibratome (Leica Vibratome VT1200S). The slices were cultured on Transwell inserts (1-μm pore size; Falcon) in neurobasal media supplemented with B27, pyruvate, and glutamine. After 24 h in culture, eHNP-A1-CD15-LDE225 (40 ng/mL) was added to the media, and then the slices were cultured for 24 h more. Subsequently, the slices were fixed in 4% paraformaldehyde and immunostained with antibodies against cleaved caspase 3 (Cell Signaling 9661). Secondary antibodies (Alexa Fluor 405 Thermo Fisher Scientific A-11012) and DAPI (Thermo Fisher Scientific D1306) were applied and confocal images were obtained using an Olympus FV1000 laser confocal microscope and captured by Olympus Fluoview Software (Integrated Cellular Imaging Core, Emory University).

In Vivo Tumor Tissue Analysis. The mouse studies were all approved by the animal care committee at Emory University. SmoA1-GFP mice ($n = 4$ for each group; saline, eHNP-A1, eHNP-A1-CD15, eHNP-A1-LDE225, and eHNP-A1-CD15-LDE225) were monitored for brain tumor symptoms based on head tilt, ataxia, and hunched posture. The needle catheters were prepared in-house by cutting 30-G needles and then inserting the cut end into 15 cm of polyethylene 10 tubing with a blunt 30-G Luer-lock hub at the end for attaching a syringe with either saline or nanoparticles dissolved in PBS or Hoechst dyes. The conscious mice were placed in a restrainer, and then the needle catheter was inserted into a lateral tail vein. Placement of the needle inside the vein was confirmed by infusing a small volume (100 to 150 μL). The mice were killed at 72 h postinjection and perfused with 4% paraformaldehyde. The perfused tissues from brain, spinal cord, liver, and tumors were harvested and immersed in 20% sucrose solution on 0.01 M PBS for 24 to 48 h. The tissues were then placed in optical cutting temperature (OCT) compound within a peel-away disposable embedding mold and transferred to a −20 °C freezer for 24 h. The frozen blocks were kept on metal grids that fit onto the cryostat (Thermo Scientific, Shandon AS620) and cryosectioned for 10-μm-thick slices. The slices were mounted on Permafrost microscope slides and immunostained before viewing under the confocal microscope. For dye

perfusion analysis, Hoechst dye and Alexa-594 conjugated lectin were injected through the tail-vein in SmoA1-GFP tumor-bearing mice and the mice were killed after 72 h. The brain, liver, spinal cord, and tumor samples were collected after perfusion with 4% paraformaldehyde and cryosectioned before observing the sections under a confocal microscope. The slices were mounted and monitored as previously described.

In Vivo Tumor Growth and Survival Monitoring. For long-term monitoring of tumor growth and survival test, two different SHH MB-bearing mouse models were used: 1) SmoA1-GFP mice treated with saline ($n = 7$) and eHNP-A1-CD15-LDE225 ($n = 6$) and 2) PTC mice treated with saline ($n = 4$) and eHNP-A1-CD15-LDE225 ($n = 4$). The MRI scans were obtained to determine the tumor volume with a 9.4 T Bio-spec scanner (Bruker). For MR imaging, mice were anesthetized with 1.5 to ~2% isoflurane during the image acquisition. Respiration, body temperature, and electrocardiogram (ECG) were monitored during the imaging. T2-weighted images were acquired using a rapid acquisition with refocused echoes (RARE) sequence in sagittal direction (time to repetition [TR] = 4,000 ms, time to echo [TE] = 42 ms, RARE factor = 8, field of view [FOV] = 20 × 20 mm^2, matrix = 116 × 116, thickness = 0.75 mm, 15 slices, and average FOV obtained per image = 12). The tumor volume was qualified as the products of slice-to-slice separation and the sum of areas from the manually drawn tumor regions of interest (ROIs) on images.

Data Availability. The authors confirm that the data supporting the findings of this study are available within the article and its supplemental materials.

ACKNOWLEDGMENTS. This work was supported by NIH National Institute of Neurological Disorders and Stroke (NINDS) R21NS091682 (Y.K.), NIH Director's New Innovator Award 1DP2HL142050 (Y.K.), National Institute on Aging R21AG056781 (Y.K.), Ian's Friends Foundation (T.J.M.), CURE Aflac Precision Medicine Program (T.J.M. and A.M.K.), Young Investigator's Award from Alex's Lemonade Stand Foundation (A.D.), and a fellowship from the Pediatric Cancer Research Foundation (Irvine, CA). A.D. and A.M.K. acknowledge support from CURE Childhood Cancer Foundation (Atlanta, GA). The content is solely the responsibility of the authors and does not necessarily represent the official views of the NIH. We would like to thank Dr. Zhihong Chen (Emory University) for consultation during blood-brain barrier experimentation and Dr. Tamara Caspary for cryotome instrumentation. We also thank the Integrated Cellular Imaging core at Emory University and the core facilities at the Parker H. Petit Institute for Bioengineering and Bioscience and the Institute for Electronics and Nanotechnology at Georgia Institute of Technology, a member of the National Nanotechnology Coordinated Infrastructure, which is supported by the NSF (ECCS-1542174).

1. P. A. Northcott *et al*., Medulloblastoma. *Nat. Rev. Dis. Primers* **5**, 11 (2019).
2. S. Rutkowski *et al*., Treatment of early childhood medulloblastoma by postoperative chemotherapy alone. *N. Engl. J. Med.* **352**, 978–986 (2005).
3. F. Bautista *et al*., Medulloblastoma in children and adolescents: A systematic review of contemporary phase I and II clinical trials and biology update. *Cancer Med.* **6**, 2606–2624 (2017).
4. S. M. Waszak *et al*., Spectrum and prevalence of genetic predisposition in medulloblastoma: A retrospective genetic study and prospective validation in a clinical trial cohort. *Lancet Oncol.* **19**, 785–798 (2018).
5. M. Kool *et al*.; ICGC PedBrain Tumor Project, Genome sequencing of SHH medulloblastoma predicts genotype-related response to smoothened inhibition. *Canc. Cell* **25**, 393–405 (2014).
6. X. Xiao *et al*., Cholesterol modification of smoothened is required for hedgehog signaling. *Mol. Cell* **66**, 154–162.e10 (2017).
7. P. Ciepla *et al*., New chemical probes targeting cholesterylation of sonic hedgehog in human cells and zebrafish. *Chem. Sci. (Camb.)* **5**, 4249–4259 (2014).
8. P. Huang *et al*., Cellular cholesterol directly activates smoothened in hedgehog signaling. *Cell* **166**, 1176–1187.e14 (2016).
9. M. Bidet *et al*., The hedgehog receptor patched is involved in cholesterol transport. *PLoS One* **6**, e23834 (2011).
10. J. B. Bell *et al*., HDL nanoparticles targeting sonic hedgehog subtype medulloblastoma. *Sci. Rep.* **8**, 1211 (2018).
11. N. J. Abbott, Blood-brain barrier structure and function and the challenges for CNS drug delivery. *J. Inherit. Metab. Dis.* **36**, 437–449 (2013).
12. N. Sukriti, *The Blood-Brain Barrier: Biology and Research Protocols*, (Humana, 2003).
13. D. R. Groothuis, The blood-brain and blood-tumor barriers: A review of strategies for increasing drug delivery. *Neuro-oncol.* **2**, 45–59 (2000).
14. L. V. Allen, N. G. Popovich, H. C. Ansel, *Ansel's Pharmaceutical Dosage Forms and Drug Delivery Systems*, (Lippincott Williams & Wilkins, ed. 8, 2006).
15. J. Bicker, G. Alves, A. Fortuna, A. Falcão, Blood-brain barrier models and their relevance for a successful development of CNS drug delivery systems: A review. *Eur. J. Pharm. Biopharm.* **87**, 409–432 (2014).
16. M. Medina-Sánchez, S. Miserere, A. Merkoçi, Nanomaterials and lab-on-a-chip technologies. *Lab Chip* **12**, 1932–1943 (2012).
17. Y. Song, J. Hormes, C. S. Kumar, Microfluidic synthesis of nanomaterials. *Small* **4**, 698–711 (2008).
18. M. Bar-Zeev, Y. D. Livney, Y. G. Assaraf, Targeted nanomedicine for cancer therapeutics: Towards precision medicine overcoming drug resistance. *Drug Resist. Updat.* **31**, 15–30 (2017).
19. J. Kim, Y. M. Lee, Y. Kang, W. J. Kim, Tumor-homing, size-tunable clustered nanoparticles for anticancer therapeutics. *ACS Nano* **8**, 9358–9367 (2014).
20. P. J. Barter *et al*., Antiinflammatory properties of HDL. *Circ. Res.* **95**, 764–772 (2004).
21. M. Navab *et al*., Mechanisms of disease: Proatherogenic HDL–An evolving field. *Nat. Clin. Pract. Endocrinol. Metab.* **2**, 504–511 (2006).
22. R. Kuai, D. Li, Y. E. Chen, J. J. Moon, A. Schwendeman, High-density lipoproteins: Nature's multifunctional nanoparticles. *ACS Nano* **10**, 3015–3041 (2016).
23. K. Y. Fung *et al*., SR-BI mediated transcytosis of HDL in brain microvascular endothelial cells is independent of Caveolin, Clathrin, and PDZK1. *Front. Physiol.* **8**, 841 (2017).
24. J. Kim, S. I. Ahn, Y. Kim, Nanotherapeutics engineered to cross the blood-brain barrier for advanced drug delivery to the central nervous system. *J. Ind. Eng. Chem.* **73**, 8–18 (2019).
25. S. Fazio, N. Pamir, HDL particle size and functional heterogeneity. *Circ. Res.* **119**, 704–707 (2016).
26. R. Movva, D. J. Rader, Laboratory assessment of HDL heterogeneity and function. *Clin. Chem.* **54**, 788–800 (2008).
27. Y. J. Sei *et al*., Detecting the functional complexities between high-density lipoprotein mimetics. *Biomaterials* **170**, 58–69 (2018).
28. S. I. Ahn *et al*., Microengineered human blood-brain barrier platform for understanding nanoparticle transport mechanisms. *Nat. Commun.* **11**, 175 (2020).
29. J. J. Link, A. Rohatgi, J. A. de Lemos, HDL cholesterol: Physiology, pathophysiology, and management. *Curr. Probl. Cardiol.* **32**, 268–314 (2007).
30. M. W. Kieran *et al*., Phase I study of oral sonidegib (LDE225) in pediatric brain and solid tumors and a phase II study in children and adults with relapsed medulloblastoma. *Neuro-oncol.* **19**, 1542–1552 (2017).
31. A. R. Hallahan *et al*., The SmoA1 mouse model reveals that notch signaling is critical for the growth and survival of sonic hedgehog-induced medulloblastomas. *Cancer Res.* **64**, 7794–7800 (2004).
32. M. Veiseh *et al*., Tumor paint: A chlorotoxin:Cy5.5 bioconjugate for intraoperative visualization of cancer foci. *Cancer Res.* **67**, 6882–6888 (2007).
33. A. Dey *et al*., YB-1 is elevated in medulloblastoma and drives proliferation in sonic hedgehog-dependent cerebellar granule neuron progenitor cells and medulloblastoma cells. *Oncogene* **35**, 4256–4268 (2016).
34. B. A. Hatton *et al*., The Smo/Smo model: Hedgehog-induced medulloblastoma with 90% incidence and leptomeningeal spread. *Cancer Res.* **68**, 1768–1776 (2008).
35. A. O. von Bueren *et al*., Treatment of young children with localized medulloblastoma by chemotherapy alone: Results of the prospective, multicenter trial HIT 2000 confirming the prognostic impact of histology. *Neuro-oncol.* **13**, 669–679 (2011).
36. S. Buonamici *et al*., Interfering with resistance to smoothened antagonists by inhibition of the PI3K pathway in medulloblastoma. *Sci. Transl. Med.* **2**, 51ra70 (2010).
37. A. Kontush, M. Lhomme, M. J. Chapman, Unraveling the complexities of the HDL lipidome. *J. Lipid Res.* **54**, 2950–2963 (2013).
38. F. H. Rached, M. J. Chapman, A. Kontush, HDL particle subpopulations: Focus on biological function. *Biofactors* **41**, 67–77 (2015).
39. W. J. M. Mulder *et al*., High-density lipoprotein nanobiologics for precision medicine. *Acc. Chem. Res.* **51**, 127–137 (2018).
40. M. J. Toth, T. Kim, Y. Kim, Robust manufacturing of lipid-polymer nanoparticles through feedback control of parallelized swirling microvortices. *Lab Chip* **17**, 2805–2813 (2017).